Journal of Power Sources 246 (2014) 32–38

Contents lists available at ScienceDirect

Journal of Power Sources

journal homepage: www.elsevier.com/locate/jpowsour

Lattice contracted Pd-hollow nanocrystals: Synthesis, structure and electrocatalysis for formic acid oxidation

Mingjun Ren [a,b], Ju Chen [a], Yuan Li [a,b], Haifeng Zhang [a], Zhiqing Zou [a], Xuemei Li [a], Hui Yang [a,*]

[a] Shanghai Advanced Research Institute, Chinese Academy of Sciences, Shanghai 201210, China
[b] University of Chinese Academy of Sciences, Beijing 100039, China

HIGHLIGHTS

- Pd-hollow/C was prepared via galvanic replacement reaction with Kirkendall effect.
- The electron transfer originally results in the lattice contraction in the hollow Pd.
- The formation of hollow structure promotes the activity for formic acid oxidation.
- The down-shift of d-band center is also origin to the enhanced activity of hollow Pd.

GRAPHICAL ABSTRACT

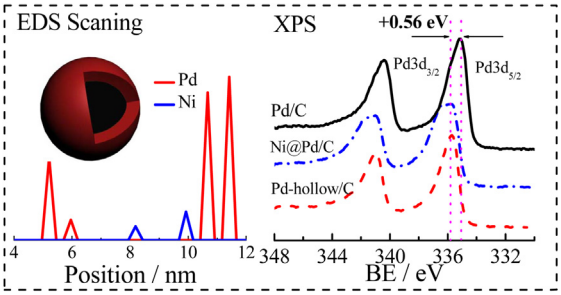

ARTICLE INFO

Article history:
Received 3 June 2013
Received in revised form
13 July 2013
Accepted 15 July 2013
Available online 25 July 2013

Keywords:
Hollow nanocrystals
Lattice contraction
Electronic structure
Electrocatalysis
Formic acid oxidation

ABSTRACT

Hollow metal nanocrystals with tuned electronic and geometric structure are highly desirable for the efficient catalytic and/or electrocatalytic reactions. Herein, we report the synthesis of carbon-supported Pd hollow nanocrystal (Pd-hollow/C) catalyst through a galvanic replacement reaction combined with Kirkendall effect without the use of polymeric stabilizer. The Pd-hollow structure is verified by scanning transmission electron microscopy. Noticeable lattice contraction in the Pd-hollow nanocrystal has been observed by high resolution transmission electron microscopy and X-ray diffraction with a decrease in the Pd (111) lattice distance. X-ray photoelectron spectroscopy indicates that the surface Pd atoms donate more electrons to the overlap with the sub-layer atoms, suggesting a strengthened d-hybridization and a down-shift of d-band center relative to the Fermi level on the surface. Electrochemical measurements show that the Pd-hollow/C catalyst exhibits a significantly enhanced electrocatalytic activity toward formic acid oxidation. The collective effects of the hollow structure and down-shift of Pd d-band center could explain well such an enhanced catalytic activity. The present study provides new insights into the relevancy of lattice parameter, electronic structure with catalytic property, and suggests design features for excellent nanostructured catalysts.

1. Introduction

Hollow structured materials, with void or yolk-like interiors, emerged and attracted much attention in the past decade [1–12]. A hollow structured material can make a minimal use of scarce, expensive materials, such as platinum and palladium, which are extensively used metals in both catalysis and electrocatalysis

* Corresponding author. Tel./fax: +86 21 20321112.
E-mail addresses: yangh@sari.ac.cn, huiyang65@hotmail.com (H. Yang).

0378-7753/$ – see front matter © 2013 Elsevier B.V. All rights reserved.
http://dx.doi.org/10.1016/j.jpowsour.2013.07.067

[1–3,12]. Generally, the enrichment of noble metals on the surface of hollow nanocrystal will result in an enhanced mass activity compared with solid nanocrystal, and thus leading to an efficient utilization of noble metals [1–3]. For example, hollow structured Pt nanocrystals showed much enhanced mass activity for the electrocatalysis of methanol oxidation as compared to Pt nanoparticles. [3] With silica sphere as template, hollow structured Pd was successfully fabricated and demonstrated an excellent catalyst for Suzuki coupling reactions. [2] Hollow structured Pd nanotubes were also prepared in Xia's group [1]. The authors claimed that such hollow structured Pd nanotubes could serve as a catalyst for highly sensitive colorimetric sensors. A more recent study observed a lattice contraction in the Pt hollow structured nanocrystal, and further investigation suggested both the hollow structure effect and lattice contraction would play some important roles in the enhancement of oxygen reduction performance [12].

Several strategies, including Kirkendall effect, Ostwald ripening, galvanic replacement reaction (GRR), and surface-protected etching, have been employed to synthesize hollow structured materials with high performance [1–11]. However, the state-of-the-art hollow structured nanocrystals based on these synthetic methods have involved either a complex route which is hard to be modulated, or massive utilization of polymeric materials as stabilizers. Polymers such as polyvinyl pyrrolidone (PVP) would strongly adsorb on the surface of nanocrystals, which could be harmful to the catalytic and/or electrocatalytic reactions. A recent study on synthesis methodology indicates that the simultaneous or sequential action of GRR and Kirkendall effect with the aid of PVP as the stabilizer could result in a precise control of both size and shape of polymetallic hollow nanocrystals with different morphology and composition. [5] Yet, the synthesis of the hollow structured nanocrystals via a simple route and without the use of polymer still remains a big challenge.

In this study, we use sodium borohydride and sodium citrate to facilitate GRR combined with Kirkendall effect to produce carbon-supported Pd-hollow nanocrystals without the use of a polymeric stabilizer. Both geometric and electronic structures of as-synthesized Pd hollow nanocrystals are investigated. Formic acid is used as a model molecule to probe the electrocatalytic properties of the Pd-hollow/C. Because the (electro)catalytic properties of nanocrystals are significantly affected by the electronic structure and lattice parameter, it is of great importance to understand the relevance of the lattice parameter and electronic structure to their catalytic property [12–14].

2. Experimental section

2.1. Preparation of catalysts

Palladium chloride ($PdCl_2$ AR), nickel nitrate ($Ni(NO_3)_2{\cdot}6H_2O$ AR), sodium borohydride ($NaBH_4$, 96%), sodium chloride (AR), sodium citrate (AR), formic acid (AR), and sulfuric acid (AR) were obtained from Sinopharm Chemical Reagent Co. Ltd (SCRC). VXC-72 carbon and 5 wt. % Nafion solution were purchased from Cabot Co. and Sigma–Aldrich, respectively.

The Pd-hollow/C was synthesized by a three-step process. All reactions were carried out under the protection of high-purity nitrogen at room temperature. To a flask was added 15 mg VXC-72 carbon, 1 mL of 0.2 M $Ni(NO_3)_2$, 20 mL of 64 mM sodium citrate, and 379 mL of water. The mixture was ultrasonicated for 30 min. Then, a freshly prepared, ice-cold $NaBH_4$ solution (0.6 M, 20 mL) was added into the above mixture within 5 min. The resultant mixture was stirred magnetically for 2 h. Thereafter, 2.5 mL of 40 mM Na_2PdCl_4 was added drop-wise into the mixture within 2 min. The mixture was stirred for another 3 h. Finally, the pH of the solution was adjusted to ca. 2 with 0.5 M H_2SO_4 and the solution was stirred for another 2 h to etch the residual Ni. The precipitates were collected by filtration and washed with ultra-pure water for three times.

The Ni@Pd/C catalyst was prepared similarly with the synthesis of Pd-hollow/C except the etching by H_2SO_4. The Pd/C catalyst was obtained by adding ice-cold $NaBH_4$ into a solution containing 15 mg VXC-72 carbon, 2.5 mL of 40 mM farther investigation suggested Na_2PdCl_4, 6.25 mL of 64 mM citrate solution, and 391 mL of ultra-pure water.

2.2. Physical characterization

XRD measurements were conducted using a Bruker D8 Advanced XRD, with Cu Kα1 radiation ($\lambda = 0.15406$ nm). The tube voltage was maintained at 40 kV and the tube current at 100 mA. Diffraction patterns were collected at a scanning rate of 2° min^{-1} and a step size of 0.02°.

TEM and HR-TEM characterization was carried out on a JEOL JEM-2100F TEM. A FEI Tecnai G2 F20 S-Twin TEM equipped with an EDS detector and a Gatan 894 CCD camera was employed for the HAADF images and EDS line analysis. The samples were prepared by ultrasonically suspending the catalyst powder in ethanol. A drop of suspension was then placed onto a holey copper grid and dried under air. The atomic composition of the catalysts was determined with an IRIS advantage inductively coupled plasma atomic emission spectroscopy (ICP-AES).

Evaluation of the electronic structure of the catalysts was conducted with an XPS (Kratos Axis Ultra^{DLD}, Britain) using Al Kα radiation. The binding energy (BE) was referenced to the C_{1s} at 284.45 eV [15].

2.3. Electrochemical evaluation of catalysts

Electrochemical experiments were carried out using Solartron Electrochemical Interface SI1287 with a standard three-electrode cell. 5 mg of the catalyst, 0.25 mL of 5 wt. % Nafion solution, and 1.25 mL of ultrapure water were mixed ultrasonically to form the catalyst ink. Subsequently, 3 μL of such a mixture was transferred onto a glassy carbon (GC, 3 mm in diameter) electrode using a microsyringe. The electrolyte used was 0.5 M H_2SO_4 or 0.5 M H_2SO_4 + 0.5 M HCOOH. High-purity nitrogen was used for the deaeration of the solutions. To determine the real ECSA of the catalyst, CVs and CO-stripping voltammograms were recorded. For the CO-stripping voltammograms, CO was pre-adsorbed at an open potential for 30 min by bubbling CO into 0.5 M H_2SO_4 solution, and then CO dissolved in solution was subsequently removed by purging high-purity N_2 for 30 min. In all cases, electrochemical measurements were conducted at a temperature of 25 ± 1 °C.

The ECSA of catalysts can be obtained by calculated the charges accumulated during the CO desorption and or H desorption [16]:

$$\mathrm{ECSA} = \frac{100 \cdot Q}{m \cdot c}$$

where Q (μC) is the charge due to the H desorption or CO desorption; c is the electrical charge associated with monolayer adsorption of H (210 μC cm^{-2}) or CO (420 μC cm^{-2}); and m is the catalyst loading on the GC electrode (10 μg).

3. Results and discussion

Morphologies of the Pd-hollow/C, Ni@Pd/C and traditional solid Pd/C are investigated using high-angle annular dark field scanning transmission electron microscopy (STEM-HAADF), and energy-dispersive X-ray spectroscopy (EDS). As shown in Fig. 1A and B,

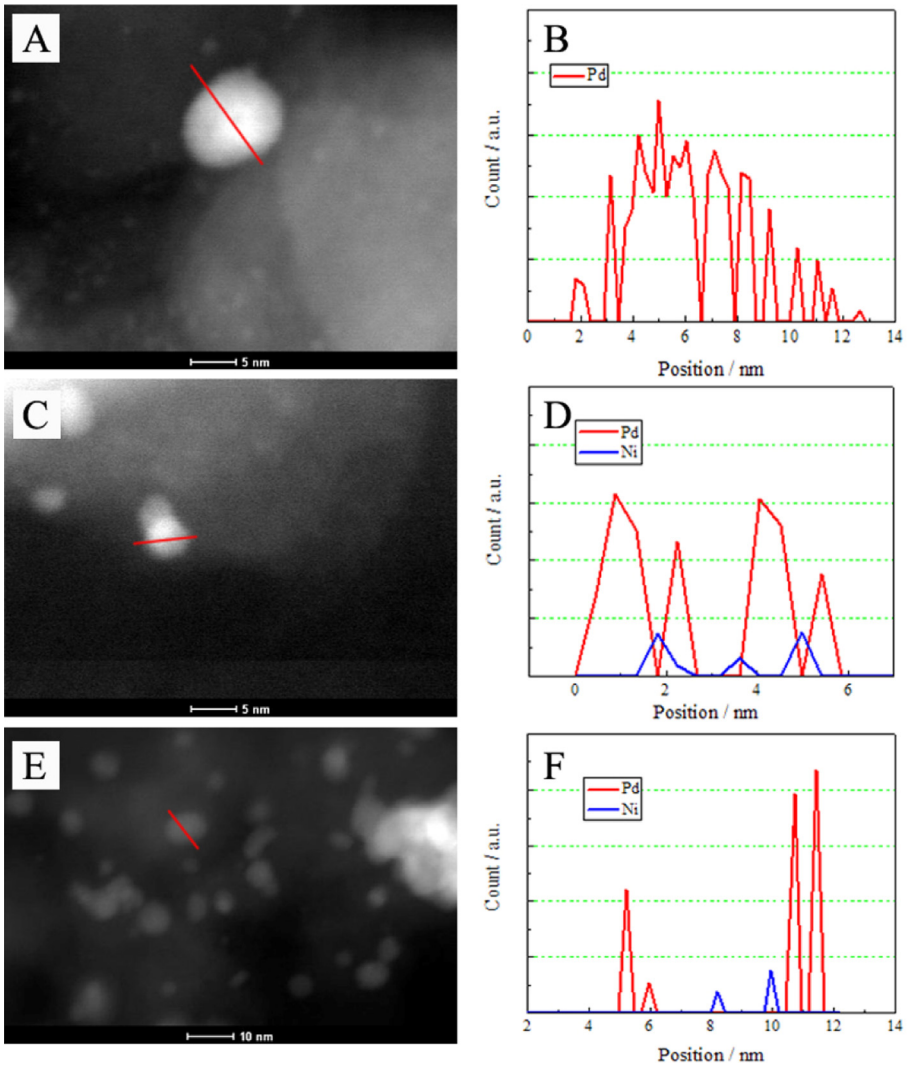

Fig. 1. STEM-HAADF overview micrographs and EDS line scan analysis along cross-section of the Pd/C (A, B), Ni@Pd/C (C, D) and Pd-hollow/C (E, F).

EDS line analysis along cross-section of an isolated metallic particle of traditional Pd/C suggests a single pump-like pattern, implying a solid sphere in the metallic nanocrystals of the Pd/C catalyst. In contrast, the Pd signals for the Ni@Pd/C and Pd-hollow/C indicate volcano-like profiles, confirming the formation of the hollow structure (Fig. 1C–F) [6–9,12]. In addition, one can clearly observe the presence of Ni atoms in both the core and shell of the Ni@Pd nanocrystals (ca. 5 wt. %, verified by inductively coupled plasma atomic emission spectroscopy, ICP-AES). Whereas the Pd-hollow shares an ignorable Ni content as evidenced by ICP-AES, implying that the etching step played a vital role in the dissolution of Ni atoms.

Fig. 2 displays the transmission electron microscopy (TEM) and high resolution transmission electron microscopy (HR-TEM) images of the Pd/C, Ni@Pd/C and Pd-hollow/C catalysts. As can be seen from Fig. 2A, C and E, the metallic nanocrystals are well dispersed on the surface of the support. The mean particle diameters based on more than 100 isolated metallic nanocrystals are ca. 7.0, 6.8 and 6.9 nm for the Pd/C, Ni@Pd/C, and Pd-hollow/C, respectively. Obviously, the three nanocrystals have the similar mean particle size. Thus, a comparison of electrocatalytic properties of the three catalysts in the following discussion would be reasonable. The observed lattice fringes belong to Pd (111) in Fig. 2B, D and E indicate a lattice spacing of 0.230, 0.223 and 0.223 nm for the Pd/C, Ni@Pd/C and Pd-hollow/C, respectively; demonstrating an obvious lattice contraction in the Ni@Pd/C and Pd-hollow/C, similar to an observation in Pt hollow nanocrystals [12].

Fig. 3 shows the XRD patterns of the Pd/C, Ni@Pd/C and Pd-hollow/C catalysts. The first diffraction peak located at ca. 30° in all XRD patterns is attributed to the carbon support. Other peaks are characteristics of the face-centered-cubic (fcc) crystalline Pd, corresponding to the facets (111), (200), (220) and (311) as marked in the figure, indicating that all the catalysts are in principle single-phased with disordered structures [15]. The mean particle diameters for the Pd/C, Ni@Pd/C, and Pd-hollow/C, as calculated from the diffraction peak (220) using Scherrer's equation, are 6.8, 6.6 and 6.7 nm, respectively. These values are slightly lower than that observed by TEM, but share the same magnitude. Interestingly, the Pd (111) diffraction peaks of the Pd-hollow/C and Ni@Pd/C nanocrystals, as shown in the inset of Fig. 3, shift to a higher 2-theta degree with a size of 0.38° relative to the same reflection in the Pd/C, clearly confirming a lattice contraction [12]. The lattice distances for the Pd/C, Ni@Pd/C and Pd-hollow/C catalysts, calculated using the (111) facets, are 0.2283, 0.2243 and 0.2238 nm, respectively. The results combined with the observation using HR-TEM clearly reveal the lattice contraction in the Pd-hollow/C and Ni@Pd/C.

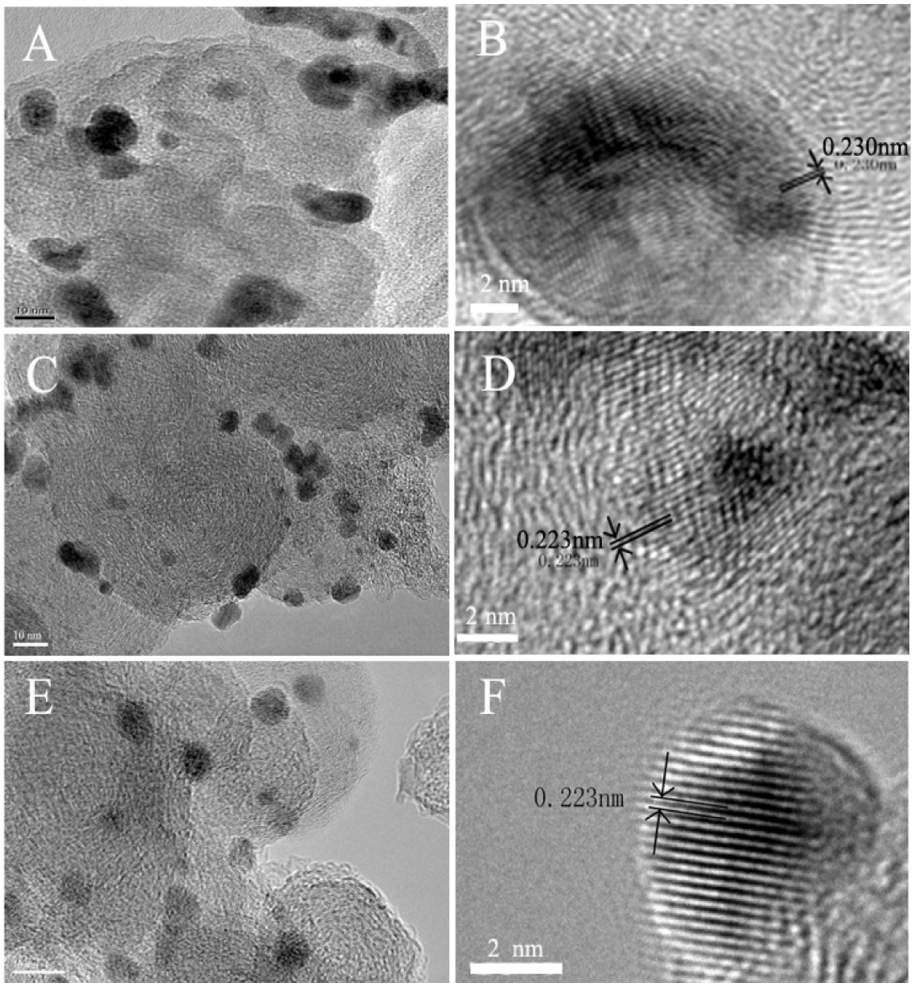

Fig. 2. TEM (scale bar: 10 nm) and HR-TEM (scale bar: 2 nm) images of the Pd/C (A, B), Ni@Pd/C (C, D) and Pd-hollow/C (E, F).

To explore the relationship between the lattice parameter and electronic structure of the Pd-hollow, X-ray photoelectron spectroscopy (XPS) was employed to investigate the electronic structure on the hollow Pd surface. As shown in Fig. 4, the Pd 3d XPS spectra split into two peaks, which can be assigned as Pd $3d_{3/2}$ and Pd $3d_{5/2}$ [15,17–20]. A dramatic surface core-level shift (SCLS) toward higher binding energy (BE) of ΔBE = +0.56 eV is observed for the Pd-hollow/C and Ni@Pd/C nanocrystals relative to the Pd/C catalyst. Given that no noticeable Pd oxides were detected on the surface, the positive SCLS is due to electrons transfer from the coordination unsaturated surface (CUS) Pd atoms to their adjacent sub-layer atoms, namely the CUS Pd atoms contribute more electrons to the d orbital overlap in the Pd-hollow/C and Ni@Pd/C relative to the

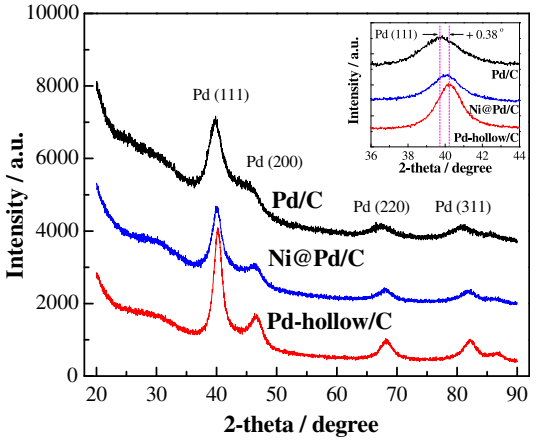

Fig. 3. XRD patterns of the Pd-hollow/C, Ni@Pd/C, and Pd/C catalysts. Inset: the magnification of the Pd (111) diffraction peak at ca. 40°.

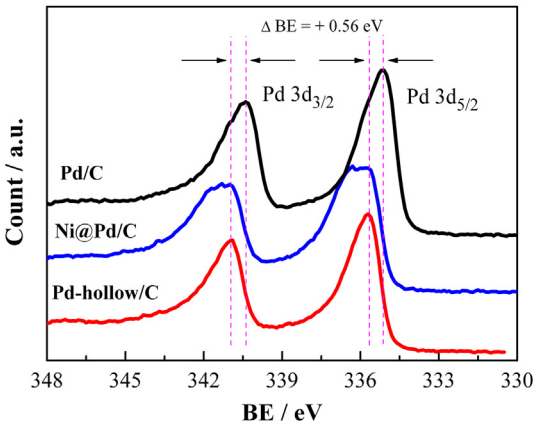

Fig. 4. XPS Pd 3d spectra of the Pd-hollow/C, Ni@Pd/C, and Pd/C catalysts.

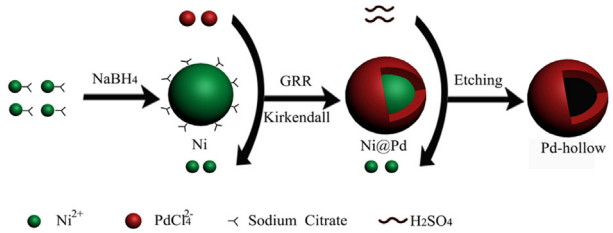

Fig. 5. Schematic diagram of protocol for the synthesis of Pd-hollow/C catalyst combined GRR and Kirkendall effect. Ni nanocrystals reduced by sodium borohydride work as sacrifice templates.

Pd/C, suggesting a strengthened Pd–Pd bond and a decreased bond length, and thus again confirming the lattice contraction within the Pd-hollow/C and Ni@Pd/C. The strengthened d-hybridization among Pd atoms of the Pd hollow will essentially lead to an increased d-band width, and thus to the down-shift of the d-band center relative to the Fermi level in order to maintain the d-band filling constant [17,18,21,22].

According to above results, the synthesis of the hollow Pd nanocrystals supported on carbon (Pd-hollow/C) can be schematically shown in Fig. 5. Generally, in a typical procedure, Ni nanocrystals were firstly obtained and subsequently served as the sacrificial template at the GRR stage owing to the lower standard reduction potential of the Ni^{2+}/Ni ($E^{\circ} = -0.257$ V vs. SHE) than that of the $PdCl_4^{2-}/Pd$ ($E^{\circ} = +0.591$ V vs. SHE). The $PdCl_4^{2-}$ ions were reduced and deposited on the surface of Ni to form the Ni@Pd yolk-shell nanocrystals supported on carbon (Ni@Pd/C). Since the Ni atoms exhibit a much higher diffusion rate compared to the Pd owing to smaller diameter, it will step across the interface between the separate bulk phase, and then transfer into the outside through the shell due to Kirkendall effect. Subsequently, the etching step using sulfuric acid leads to a quick dissolution of the Ni atoms in the shell, yielding hollow Pd nanocrystals supported on carbon (Pd-hollow/C) [5,6,10].

Based on above observations, it is concluded that the formation of hollow Pd nanocrystals leads to a lattice contraction in the crystal, which directly promotes the electron transfer from surface to the sub-layer, and subsequently to the positive SCLS as well as the down-shift of the d-band center [14,23,24]. It is expected that both the structural effect due to the formation of hollow structure and down-shift of d-band center would promote the catalytic activity of Pd-hollow/C in some special systems. To probe the electrocatalytic property of the Pd-hollow/C, Fig. 6 presents the cyclic voltammograms and CO-stripping profiles of the Pd-hollow/C, Ni@Pd/C and Pd/C in 0.5 M H_2SO_4 solution with all the currents normalized to the geometric area of the GC. As can be seen in Fig. 6A, all the catalysts show the typical hydrogen and oxygen adsorption/desorption region of metallic Pd. The adsorbed CO oxidation peaks on the three catalysts are centered at ca. 0.65 V (vs. SCE), as shown in Fig. 6B. By calculating the hydrogen desorption region area, the specific electrochemical surface area (ECSA) are estimated as 10.17, 7.57 and 15.14 $m^2\ g^{-1}$ for the Pd/C, Ni@Pd/C and Pd-hollow/C catalysts, respectively. Similarly, the ECSAs for the Pd/C, Ni@Pd/C and Pd-hollow/C catalysts calculated from CO oxidation peaks in Fig. 6B are 8.24, 7.20 and 14.07 $m^2\ g^{-1}$, respectively; as listed in Table 1. One can observe an increase in ECSA based on CO oxidation peaks by factors of 94.9% and 70.2% for the Pd-hollow/C relative to the Ni@Pd/C and Pd/C, revealing an efficient utilization of the Pd atoms in the Pd-hollow/C catalyst. Hence, we deduce that the increased ECSA of the Pd-hollow/C is mainly due to the structure effect by the formation of Pd hollow structure which leads to an increased CUS per mass metal. Most interestingly, the onset

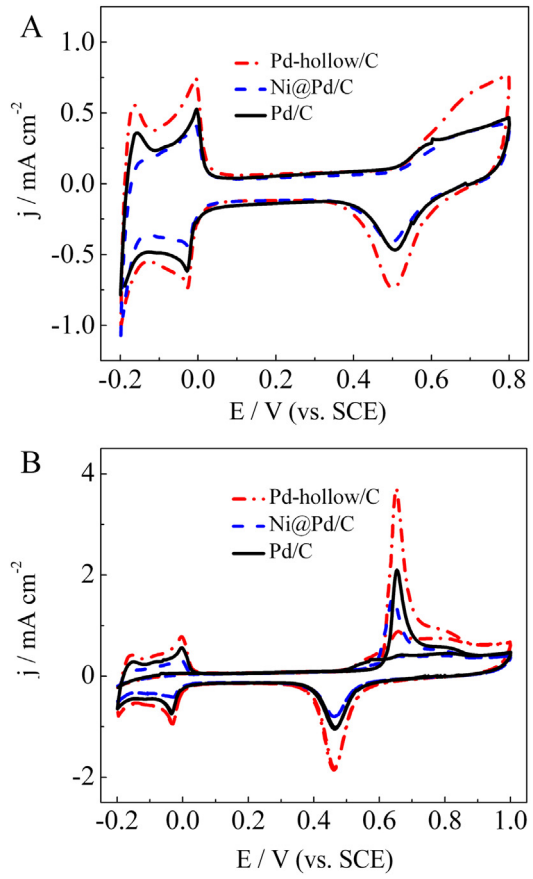

Fig. 6. Cyclic voltammograms (A) and CO-stripping (B) profiles of the Pd-hollow/C (red dash dot), Ni@Pd/C (blue dash) and Pd/C (black solid) in 0.5 M H_2SO_4 at a scan rate of 20 mV s^{-1}. (For interpretation of the references to color in this figure legend, the reader is referred to the web version of this article.)

oxidation potential for CO_{ads} on the Pd-hollow/C and Ni@Pd/C shows a slightly negative shift relative to that on the Pd/C. Generally, in a typical surface–CO_{ads} interaction system, when electrons are donated from CO 5σ to the CUS atoms and donate back from the CUS d state to the 2π*, the down-shift of d-band center means a reduced 2π* back-donation, thereby leading to weaker surface–CO bonds [14,21,25–29]. In this case, the formation of oxygen-containing species would also be weakened [13]. Since the removal of CO_{ads} needs to react with the adsorbed oxygen-containing species. Thus, due to the collective effects, the onset potential for CO_{ads} oxidation exhibits only slightly negative shift.

To evaluate the electrocatalytic activity toward formic acid oxidation, the electrodes were transferred into 0.5 M H_2SO_4 + 0.5 M HCOOH solution. Fig. 7 shows cyclic voltammograms and *i*–*t* amperometric curves of the Pd-hollow/C, Ni@Pd/C and Pd/C catalysts in nitrogen-saturated 0.5 M H_2SO_4 + 0.5 M HCOOH. From Fig. 7A, the maximum current densities for formic acid oxidation decrease in the order of Pd-hollow/C > Pd/C > Ni@Pd/C, which is in fairly good agreement with the ECSA, suggesting that the formation

Table 1
The ECSA and current density of formic acid oxidation at 0.16 V (j@0.16 V).

Sample	ECSA(H)/$m^2\ g^{-1}$	ECSA(CO)/$m^2\ g^{-1}$	j@0.16 V/mA cm^{-2}
Pd/C	10.17	8.24	12.38
Ni@Pd/C	7.57	7.20	20.24
Pd-hollow/C	15.14	14.03	34.38

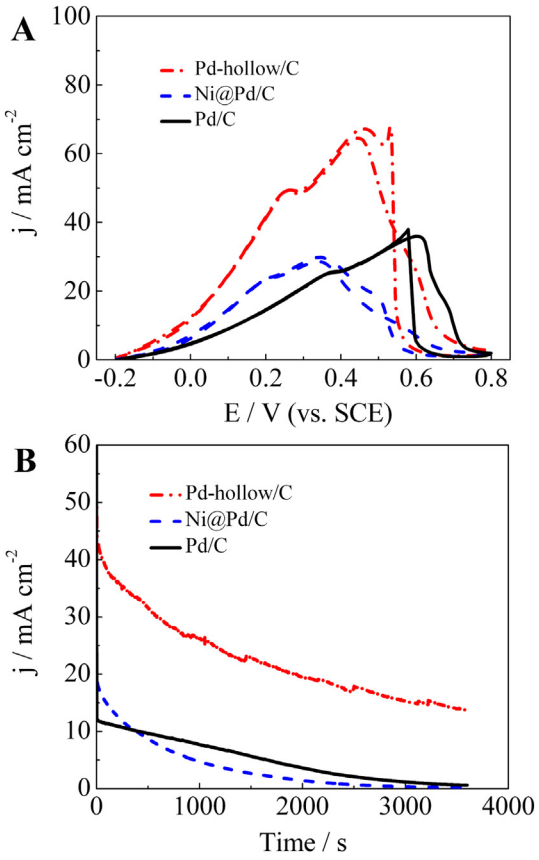

Fig. 7. Cyclic voltammograms (A; scan rate: 50 mV s^{-1}) and amperometric i–t curves (B; 0.16 V vs. SCE) of the Pd-hollow/C (red dash dot), Ni@Pd/C (blue dash) and Pd/C (black solid) in nitrogen-saturated 0.5 M H_2SO_4 + 0.5 M HCOOH. (For interpretation of the references to color in this figure legend, the reader is referred to the web version of this article.)

of hollow structure play an important role in performance enhancement. Importantly, the formic acid oxidation peaks on the Pd-hollow/C and Ni@Pd/C shifts negatively relative to that on the Pd/C, implying that formic acid adsorbed on the Pd-hollow/C and Ni@Pd/C can be removed easier than that on the Pd/C. This can be ascribed to the change in the electronic structure, which involves the strength of adsorption bonds [14]. Such a result is consistent with previous report that the down-shift of the d-band center would improve the catalytic performance of formic acid oxidation on Pd-based catalysts [5,14]. In addition, the current density at 0.16 V (vs. SCE) on the Pd-hollow/C is about 1.7 and 2.8 times higher than that on the Ni@Pd/C and Pd/C, again evidencing a significantly enhanced catalytic activity toward the formic acid oxidation (cf. Table 1). One can find that the comparison of current densities at 0.16 V demonstrated a different order with the maximum current densities on the three catalysts, implying that a variation in the electronic structure, in cooperation with the structure effect, has played a role in promoting the electrocatalytic activities. Furthermore, the current densities collected at 0.16 V (vs. SCE) for 1 h illustrates the same trend with the above findings at 0.16 V at the very start. However, such a trend is similar to the comparison of maximum current densities due to the degradation on Ni@Pd/C catalyst ca. 5 min later, as can be seen in Fig. 7B. We have also conducted the synthesis of hollow structure Pd nanocrystal with the aid of PVP as stabilizer. However, its electrocatalytic activity for formic acid oxidation is much lower than that on the Pd hollow/C without the use of PVP in this work, probably due to the presence of residence PVP.

The above findings consistently suggest that much enhanced electrocatalytic activity of the Pd-hollow/C relative to traditional Pd/C toward the formic acid oxidation. Two reasons might account for such an enhanced catalytic activity on the Pd-hollow/C. One is the favorable structure effect. Hollow structure leads to an increased CUS, which plays a crucial role in promoting mass activity of Pd [12]. The other is the down-shift of d-band center of the Pd hollow nanocrystals, which induced lower overpotential of formic acid oxidation on the Pd-hollow/C as compared to Pd/C [14]. A recent research also suggests that Pd with a low 3d electron density binds hardly to the $-COOH_{ads}$ intermediate and subsequently the $-COOH_{ads}$ surface coverage is reduced, thus leading to formic acid oxidation easily via a direct pathway to final product carbon dioxide [18,19].

4. Conclusions

A Pd-hollow/C catalyst has been successfully synthesized via a GRR combined with Kirkendall effect without the use of polymeric stabilizer. Lattice contraction and electron transfer from the surface Pd atoms to the adjacent sub-layer atoms have been verified in the Pt-hollow/C. The electrocatalytic activity of the Pd-hollow/C toward the formic acid oxidation is much enhanced over the solid Pd/C, and the formic acid oxidation peak on the Pd-hollow/C shifts negatively relative to that on the Pd/C. The increase in the CUS Pd atoms due to the formation of hollow structure, as well as the down-shift of the d-band center in the Pd-hollow/C could explain the improved electrocatalytic activity of formic acid oxidation. The present research provides new insights to design and synthesize nanostructured catalysts with expectation properties.

Acknowledgments

We are grateful for the partial financial support from the National Basic Research Program of China (973 Program) (2012CB 932800), the Natural Science Foundation of China (21073219), Shanghai Science and Technology Committee (11DZ1200400), the Knowledge Innovation Engineering of the CAS (12406, 124091231), and the Scientific and Technological Innovation Fund for Graduate Student of the CAS.

References

[1] Y.G. Sun, B. Mayers, Y.N. Xia, Adv. Mater. 15 (2003) 641.
[2] S.W. Kim, M. Kim, W.Y. Lee, T. Hyeon, J. Am. Chem. Soc. 124 (2002) 7642.
[3] H.P. Liang, H.M. Zhang, J.S. Hu, Y.G. Guo, L.J. Wan, C.L. Bai, Angew. Chem. Int. Ed. 43 (2004) 1540.
[4] Y.D. Yin, R.M. Rioux, C.K. Erdonmez, S. Hughes, Science 304 (2004) 711.
[5] E. Gonzalez, J. Arbiol, V.F. Puntes, Science 334 (2011) 1377.
[6] Y. Lu, Y. Zhao, L. Yu, L. Dong, C. Shi, M.J. Hu, Y.J. Xu, L.P. Wen, S.H. Yu, Adv. Mater. 22 (2010) 1407.
[7] L.J. Lauhon, M.S. Gudiksen, D. Wang, C.M. Lieber, Nature 420 (2002) 57.
[8] H.L. Jiang, Q. Xu, J. Mater. Chem. 21 (2011) 13705.
[9] F. Wang, R.R. Deng, J. Wang, Q.X. Wang, Y. Han, H.M. Zhu, X.Y. Chen, X.G. Liu, Nat. Mater. 10 (2011) 968.
[10] S.E. Skrabalak, L. Au, X.D. Li, Y.N. Xia, Nat. Protoc. 2 (2007) 2182.
[11] W.S. Wang, M. Dahl, Y.D. Yin, Chem. Mater. 25 (2013) 1179.
[12] J.X. Wang, C. Ma, Y.M. Choi, D. Su, Y.M. Zhu, P. Liu, R. Si, M.B. Vukmirovic, Y.R. Zhang, R. Adzic, J. Am. Chem. Soc. 133 (2011) 13551.
[13] P. Strasser, S. Koh, T. Anniyev, J. Greeley, K. More, C.F.Z. Yu, C. Liu, S. Kaya, D. Nordlund, H. Ogasawara, M.F. Toney, A. Nilsson, Nat. Chem. 2 (2010) 454.
[14] L.A. Kibler, A.M. El-Aziz, R. Hoyer, D.M. Kolb, Angew. Chem. Int. Ed. 44 (2005) 2080.
[15] M.J. Ren, Y.Y. Kang, W. He, Z.Q. Zou, X.Z. Xue, D.L. Akins, H. Yang, S.L. Feng, Appl. Catal. B: Environ. 104 (2011) 49.
[16] S. Zhang, Y.Y. Shao, G.P. Yin, Y.H. Lin, Angew. Chem. Int. Ed. 49 (2010) 2211.
[17] W.J. Zhou, J.Y. Lee, J. Phys. Chem. C 112 (2008) 3789.
[18] W.P. Zhou, A. Lewera, R. Larsen, R.I. Masel, P.S. Bagus, A. Wieckowski, J. Phys. Chem. B 110 (2006) 13393.
[19] G.X. Yang, Y. Chen, Y.M. Zhou, Y.W. Tang, T.H. Lu, Electrochem. Commun. 12 (2010) 492.

[20] G. Ketteler, D.F. Ogletree, H. Bluhm, H.J. Liu, E.L.D. Hebenstreit, M. Salmeron, J. Am. Chem. Soc. 127 (2005) 18269.
[21] Y.Y. Tong, H.S. Kim, P.K. Babu, P. Waszczuk, A. Wieckowski, E. Oldfield, J. Am. Chem. Soc. 124 (2002) 468.
[22] J.R. Kitchin, J.K. Nørskov, M.A. Barteau, J.G. Chen, Phys. Rev. Lett. 93 (2004) 156801.
[23] B. Richter, H. Kuhlenbeck, H.-J. Freund, P.S. Bagus, Phys. Rev. Lett. 93 (2004) 026805.
[24] M. Mavrikakis, B. Hammer, J.K. Nørskov, Phys. Rev. Lett. 81 (1998) 2819.
[25] J.K. Nørskov, T. Bligaard, J. Rossmeisl, C.H. Christensen, Nat. Chem. 1 (2009) 37.
[26] B. Hammer, Y. Morikawa, J.K. Nørskov, Phys. Rev. Lett. 76 (1996) 2141.
[27] T. Bligaard, J.K. Nørskov, Electrochim. Acta 52 (2007) 5512.
[28] A. Ruban, B. Hammer, P. Stoltze, H.L. Skriver, J.K. Nørskov, J. Mol. Catal. A: Chem. 115 (1997) 421.
[29] G. Ertl, Angew. Chem. Int. Ed. 15 (1976) 391.